Available online at www.sciencedirect.com
ScienceDirect
Acta Materialia 58 (2010) 4772–4782
Acta MATERIALIA
www.elsevier.com/locate/actamat

In situ TEM study of microplasticity and Bauschinger effect in nanocrystalline metals

Jagannathan Rajagopalan [a], Christian Rentenberger [b], H. Peter Karnthaler [b], Gerhard Dehm [c], M. Taher A. Saif [a,*]

[a] Mechanical Science and Engineering Department, University of Illinois at Urbana-Champaign, 1206 W Green Street, Urbana, IL 61801, USA
[b] Physics of Nanostructured Materials, Faculty of Physics, University of Vienna, Boltzmanngasse 5, A-1090 Wien, Austria
[c] Erich Schmid Institute of Materials Science, Austrian Academy of Sciences, and Dept. Materials Physics, University of Leoben, Jahnstr.12, 8700 Leoben, Austria

Received 11 March 2010; received in revised form 3 May 2010; accepted 4 May 2010
Available online 9 June 2010

Abstract

In situ transmission electron microscopy straining experiments with concurrent macroscopic stress–strain measurements were performed to study the effect of microstructural heterogeneity on the deformation behavior of nanocrystalline metal films. In microstructurally heterogeneous gold films (mean grain size $d_m = 70$ nm) comprising randomly oriented grains, dislocation activity is confined to relatively larger grains, with smaller grains deforming elastically, even at applied strains approaching 1.2%. This extended microplasticity leads to build-up of internal stresses, inducing a large Bauschinger effect during unloading. Microstructurally heterogeneous aluminum films ($d_m = 140$ nm) also show similar behavior. In contrast, microstructurally homogeneous aluminum films comprising mainly two grain families, both favorably oriented for dislocation glide, show limited microplastic deformation and minimal Bauschinger effect despite having a comparable mean grain size ($d_m = 120$ nm). A simple model is proposed to describe these observations. Overall, our results emphasize the need to consider both microstructural size and heterogeneity in modeling the mechanical behavior of nanocrystalline metals.

Keywords: Nanocrystalline materials; Plastic deformation; Yield phenomena; Microstructural heterogeneity; Thin films

1. Introduction

The deformation behavior of nanocrystalline metals, which typically have mean grain sizes around 100 nm or less, has attracted extensive interest in recent years. Unlike coarse-grained polycrystalline solids, where plasticity is dominated by dislocations generated by intragranular dislocation sources [1], alternative deformation mechanisms can be activated in nanocrystalline metals due to the paucity of intragranular dislocation sources and the difficulty in activating them [2,3]. The alternative deformation mechanisms include grain boundary (GB) diffusion and sliding [4], GB migration [5], twinning [6] and grain rotation [7]. As a result, nanocrystalline metals exhibit several unusual characteristics, such as high strength [8], high strain rate sensitivity [9,10] and stress-induced room temperature grain growth [11,12].

Molecular dynamics (MD) simulation has been one of the most widely used approaches to model deformation processes in nanocrystalline metals [13,14]. MD simulations suggest that plasticity in nanocrystalline metals is carried by partial dislocations nucleated at GBs; in materials such as Cu and Ni only one partial is emitted, leading to the formation of stacking faults, whereas in Al a trailing partial follows, resulting in a twin or a full dislocation [15]. Recent studies [16], though, have emphasized the need to consider the constraints in MD simulations, such as the small time scales, in interpreting these results. Qualitative in situ transmission electron microscopy (TEM) [17–19] has been

* Corresponding author. Tel.: +1 217 333 8552; fax: +1 217 244 6534.
E-mail address: saif@illinois.edu (M.T.A. Saif).

1359-6454/$36.00
doi:10.1016/j.actamat.2010.05.013

another major technique used to probe deformation mechanisms in nanocrystalline metals. These studies have shown that dislocation-mediated plasticity continues to be a dominant mechanism in nanocrystalline metals with mean grain sizes above 30 nm. In single crystal gold films, transition from perfect to partial dislocation plasticity has been observed at a thickness of 80 nm [20]. However, despite the tremendous advances in the modeling and experimental characterization [21], some major aspects of the deformation behavior of nanocrystalline metals still remain unclear.

One such aspect is the elastic–plastic transition and the macroscopic yielding of nanocrystalline metals. In coarse-grained metals the macroscopic yield stress is usually defined by the stress at 0.2% offset strain, with the assumption that the majority of the grains are deforming plastically at this point. So far, this criterion has largely been applied to determining and comparing the yield stresses of nanocrystalline metals. However, recent reports have revealed a significantly extended microplastic regime in nanocrystalline metals and questioned the validity of this yield criterion [22,23]. To account for the extended microplasticity, a tangent modulus-based approach [24,25] to determine the elastic–plastic transition has been suggested. Combining such an approach with in situ X-ray diffraction experiments, a new criterion for yielding in nanocrystalline metals has recently been proposed [26].

Another aspect that has received relatively little attention is the effect of microstructural heterogeneity on the deformation behavior of metals in the nanocrystalline transition regime (mean grain size between 50 and 150 nm). This is surprising, since nanocrystalline metals synthesized by severe plastic deformation often have grain sizes in this regime and are known to have a highly heterogeneous microstructure [27]. Understanding the relationship between microstructural heterogeneity and the deformation behavior is especially relevant since recent investigations [28,29] have revealed that the unusual plastic strain recovery in nanocrystalline metals [30,31] is a direct consequence of microstructural heterogeneity. However, a detailed mechanistic understanding of how microstructural heterogeneity influences the mechanical behavior is still lacking. TEM experiments allow such mechanistic investigations, provided the macroscopic material response is measured while the microstructure is visualized. Until now, such studies have been limited due to the lack of appropriate instrumentation.

In this work, we studied how microstructural heterogeneity affects the deformation behavior of nanocrystalline metal films (mean grain size 70–140 nm) in which dislocation-mediated plasticity dominates. Towards this end, we synthesized free-standing nanocrystalline gold and aluminum films with highly dissimilar microstructures and performed in situ TEM straining experiments with concurrent macroscopic stress–strain measurements. Our experiments show that the extent of microplasticity as well as the overall deformation response of nanocrystalline metals is strongly influenced by heterogeneity. The gold films, which have a heterogeneous microstructure, show large microplastic deformation and do not yield macroscopically even at 1.2% applied strain. In contrast, the microstructurally homogeneous aluminum films show limited microplastic deformation and a markedly sharper elastic–plastic transition. Furthermore, our experiments reveal the mechanism for the unusual Bauschinger effect observed in free-standing metal films [32].

2. Experimental details

A 160 nm thick gold film and a 225 nm thick aluminum film were sputter deposited on Si (0 0 1) wafers. Before deposition, the native silicon dioxide layer on the Si wafers was removed by hydrofluoric acid etching and the wafers were immediately transferred to the sputtering chamber to avoid regrowth of the oxide layer. From these wafers, free-standing gold and aluminum tensile specimens were co-fabricated with microtensile devices using the process described in Ref. [33].

The thickness of the thin film specimens fabricated using this process is highly uniform, with a variation of less than 5 nm, unlike conventional TEM samples. In addition, these tensile testing devices ensure uniform uniaxial loading and unloading of the specimen and eliminate bending and torsion to a large extent [34]. They are also compatible with the standard TEM straining specimen holders, and have built-in force and displacement sensors that allow the measurement of the macroscopic stress and strain during in situ straining. This allows us to directly relate the microstructural changes during deformation to the macroscopic behavior and thus establish the structure–property relationship. The maximum strain that can be imposed on the thin film specimens with these devices is around 6–7%, which precludes the observation of very large ductility in our specimens. However, this is not usually a limitation because the failure strain does not exceed 2% in majority of the specimens. The relatively low failure strain is due partly to the large aspect ratio of the specimens (length 350 μm, thickness 150–250 nm) and partly to flaws introduced during the fabrication.

Uniaxial tensile load–unload experiments were performed using a displacement controlled, single tilt, straining specimen holder in a Philips CM200 transmission electron microscope at an accelerating voltage of 200 kV. The loading and unloading on both the gold and aluminum specimens were performed in a series of steps; a set of two to three displacement pulses (strain of ≈0.05–0.1%) were imposed and the evolution of the microstructure was observed for a period of a few minutes at constant displacement. During all cycles, the microstructural observations were made under bright field conditions and recorded using a real-time TV-rate camera (30 frames per second) with an image intensifier.

In the case of the gold specimen, grains with favorable orientation for dislocation glide were identified before straining using the following procedure: dark-field images were taken using diffraction spots that were aligned parallel

to the straining direction. In the case of dark-field images with [2 0 0] reflections parallel to the straining direction, for example, grains having slip systems with a large Schmid factor show up. Using this procedure and convergent beam diffraction methods, a relatively large grain (indicated as "A" in Fig. 3a) that was favorably oriented for dislocation glide and surrounded by smaller grains was selected for imaging. In the aluminum specimen, since all the grains had a similar Schmid factor (for reasons described below), no effort was taken to identify favorably oriented grains.

3. Microstructural characterization

The microstructure of the thin film specimens were examined using TEM and X-ray diffraction. The gold film did not show epitaxial growth and had a fairly heterogeneous microstructure (Fig. 1a), with a weak [1 1 1] texture in the film growth direction and a uniform in-plane texture. The average grain size (d_m) was 70 nm, but some very small grains ($<0.2d_m$) and some fairly large grains ($\approx 2.5d_m$) were also present (Fig. 1b). Such a wide distribution of grain sizes has been observed previously in other nanocrystalline metals and alloys [35].

The aluminum film ($d_m = 120$ nm) showed a less pronounced variation (Fig. 1d) between the smallest grains ($\approx 0.5d_m$) and the largest ($\approx 2.5d_m$). More importantly, the film showed epitaxial growth [36] with the following relationships: Al(1 1 0)||Si(0 0 1), Al[0 0 1]||Si[1 1 0] and Al(1 1 0)||Si(0 0 1), Al[0 0 1]||Si[1 $\bar{1}$ 0]. In other words, the film had a fairly homogeneous microstructure with a strong (1 1 0) out-of-plane texture and only two in-plane grain orientations, rotated 90° in-plane with respect to each other. Because the tensile loading axis was aligned with the [0 0 1] direction of one set of grains and the [1 $\bar{1}$ 0] direction of the other set, all the grains had several [1 1 0]{1 1 1} slip systems with an identical Schmid factor of 0.408. This drastically reduced the plastic incompatibilities that can arise from variations in resolved shear stresses in different grains.

4. Experimental results

4.1. In situ TEM deformation of nanocrystalline gold film with heterogeneous microstructure

The stress–strain response of the gold film during in situ TEM deformation is shown in Fig. 2a. In the first two

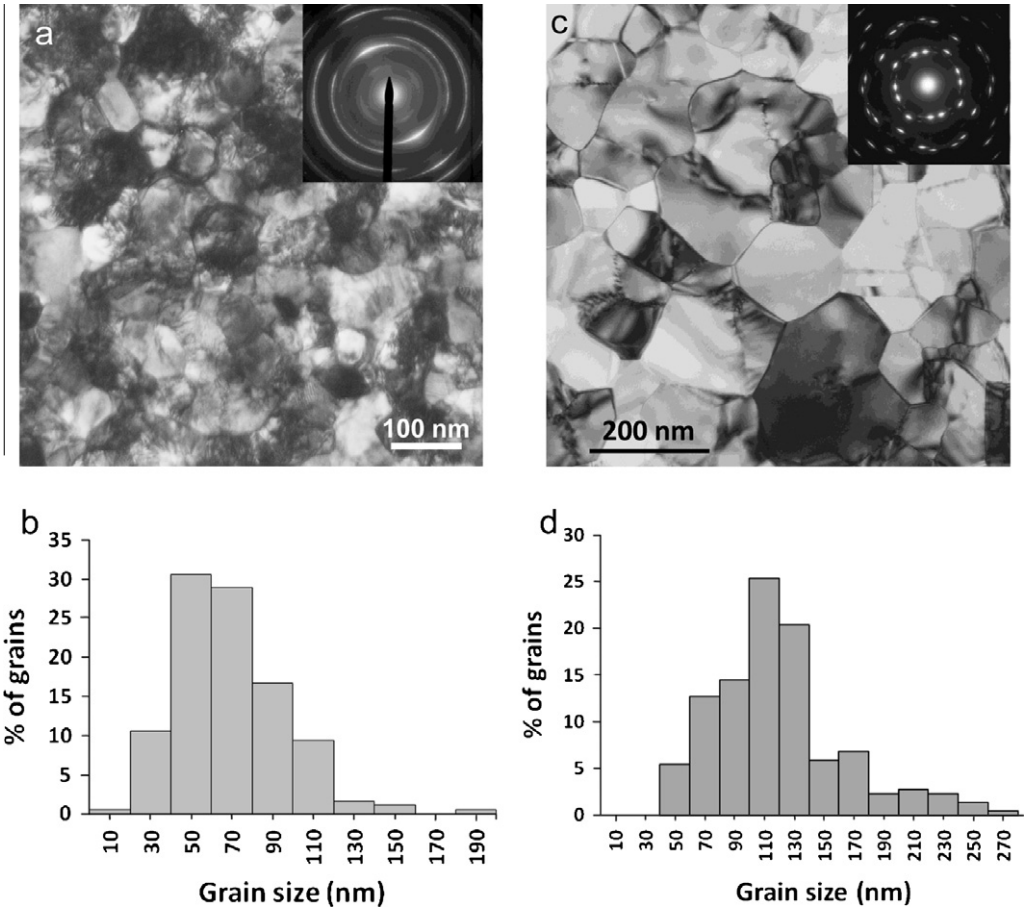

Fig. 1. Bright-field transmission electron micrograph (a) and histogram of the grain size distribution (b) of the gold film. Bright-field transmission electron micrograph (c) and histogram of the grain size distribution (d) of the aluminum film. The aluminum film has only two (1 1 0) growth variants, rotated 90° with respect to each other. The corresponding diffraction patterns (shown as insets in (a) and (c)) reveal the different texture of the two films.

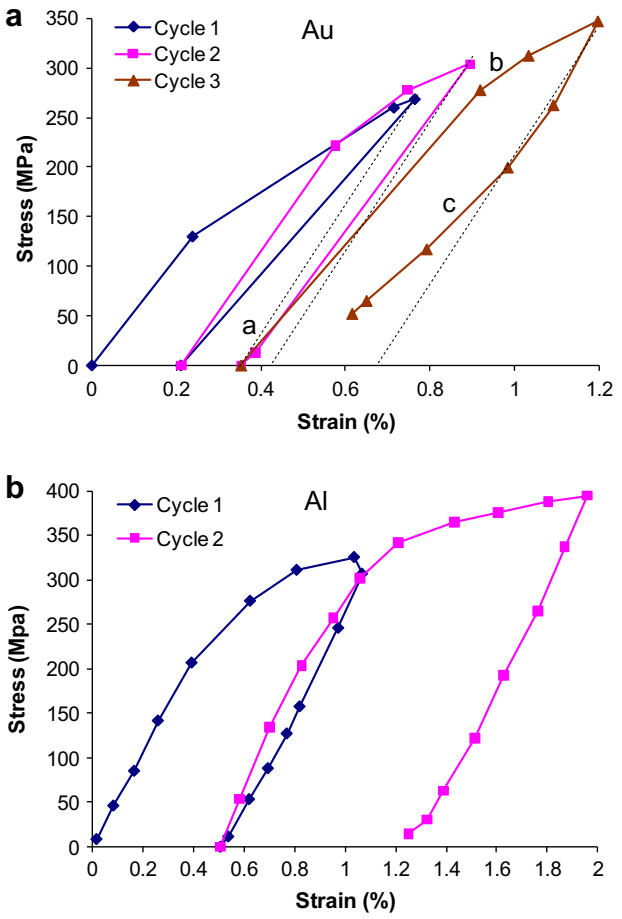

Fig. 2. (a) The stress–strain measurements for the gold film during in situ TEM deformation. Note that the stress–strain curves deviate from the elastic unloading path (indicated by dashed black lines) during all three deformation cycles. In the first and second cycles, stress–strain measurements were made at only a few points, whereas the third cycle was recorded in more detail. The microstructural changes that accompany strain increments/decrements during stages a–c of the third deformation cycle are shown in Fig. 4 (see text for details). (b) The stress–strain measurements for the aluminum film during in situ TEM deformation, showing a fairly sharp elastic–plastic transition.

deformation cycles, we focused mainly on identifying the deformation mechanisms and qualitatively observing the microstructural changes. During the third cycle, stress–strain measurements were made regularly to correlate the changes in the microstructure with the macroscopic behavior. The measurements provide direct evidence of the macroscopic Bauschinger effect, as seen by the pronounced deviation of the stress–strain response from elastic behavior during unloading.

Fig. 3 shows the time evolution of the microstructure in the gold specimen after the application of a set of deformation pulses towards the end of loading in the third cycle (for the corresponding movie, see Video S1; note that this video, as well as Videos S2, S3 and S4, are played at four times the actual speed). As evident from the images, dislocation-induced changes in contrast (indicated by red arrows) were confined to only a few grains, with especially high activity in the large grain in the middle. No noticeable dislocation activity was seen in most of the smaller grains, which indicates that the smaller grains are deforming elastically (for more evidence of such elastic–plastic deformation see Video S2). In other words, the gold specimen shows microplastic deformation even though the plastic strain induced in this cycle (>0.3%) is well above the conventional 0.2% limit for the macroplastic transition. It is likely, however, that the dislocation activity in some of the smaller grains was missed due to unfavorable diffraction conditions or the short time scales for dislocation motion in them.

Furthermore, even with the applied displacement held constant, dislocation bursts continued to occur several minutes after the initial deformation pulse. This phenomenon, which was seen during all three deformation cycles, indicates a thermal dependence of dislocation propagation by depinning events and may explain the high strain rate sensitivity observed in nanocrystalline metals [10]. The sequence of video frames shown in Fig. 3d–f shows the nucleation and propagation of a dislocation from the upper left GB of the large grain. During its propagation, this dislocation gets pinned at one of its ends and further propagation occurs upon depinning. Such time-dependent depinning of dislocations at GBs has been observed previously in MD simulations and was shown to be a thermally activated process [37]. We note that in all our analysis only sudden contrast changes, as opposed to changes caused by elastic distortions, were interpreted as a signature of dislocation activity. In most cases, these sudden contrast changes were accompanied by visible motion of dislocations.

This extended microplasticity during loading offers a straightforward explanation for the Bauschinger effect seen during unloading. During the initial stages of loading (Fig. 4a) there were no changes in contrast in any of the grains, indicating that the deformation is primarily elastic. However, with increasing strain sudden changes in contrast, frequently accompanied by visible motion of individual dislocations, were observed in the larger grain (Fig. 4b) but were largely absent in the surrounding smaller grains. Furthermore, the onset of dislocation activity in the larger grain coincides with a reduction in the macroscopic stress–strain slope, which suggests that the apparent high strain hardening is just a manifestation of this elastic–plastic deformation. More importantly, the plastic relaxation leads to a lower stress level in the larger grain as compared to its elastically deforming neighbors, leading to a build-up of internal stresses.

During the initial phase of unloading, contrast changes were not seen in any of the grains, which is consistent with the observed elastic stress–strain response. However, upon further unloading, the dislocation configuration in the larger grain became unstable and noticeable dislocation activity was seen after an unloading pulse (Fig. 4c). Similar dislocation activity was observed intermittently as the unloading progressed. Since the macroscopic stress reduces

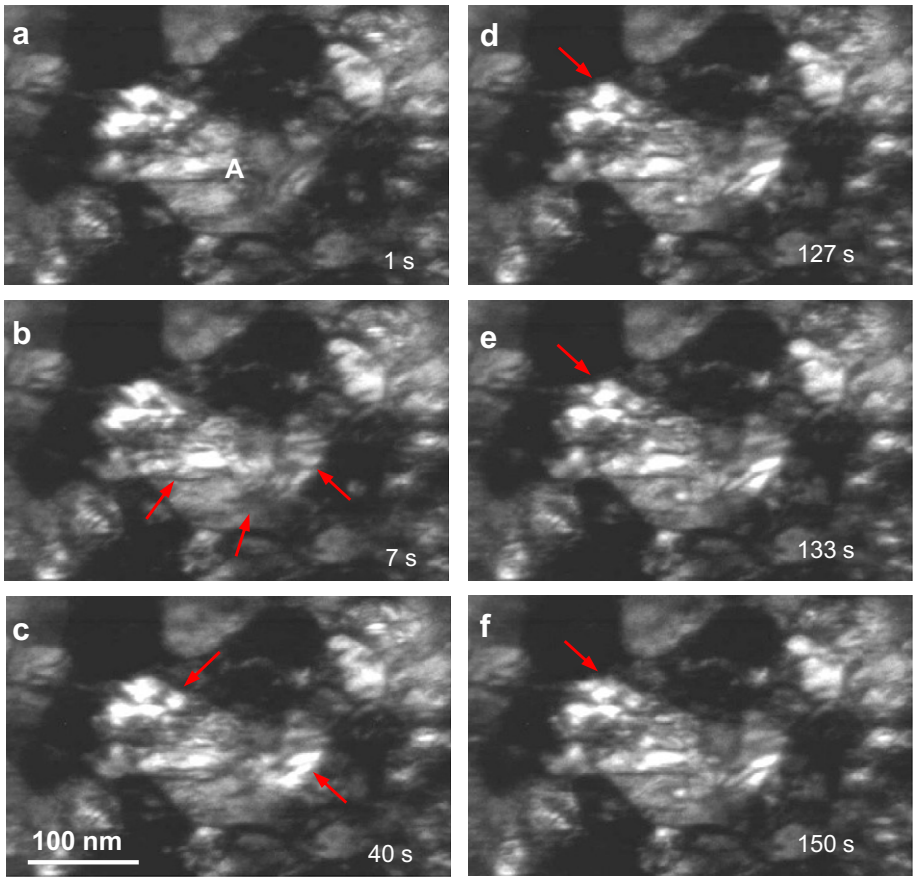

Fig. 3. The time evolution of microstructure of the gold film at the end of the third loading cycle (total strain 1.1%) with the applied displacement held constant (for the corresponding movie see Video S1). Figs. (a)–(c) show that the dislocation-induced changes in contrast (indicated by red arrows) were primarily restricted to the large grain in the middle. Figs. (d)–(f) show a special case of a dislocation nucleation and propagation. The snapshot at $t = 127$ s shows the dislocation nucleating from the upper left GB of the large grain. The snapshots at $t = 133$ s and $t = 150$ s show the dislocation being pinned at the GB during its propagation. (For interpretation of the references to colour in this figure legend, the reader is referred to the web version of this article.)

with each unloading pulse, this dislocation activity appears to result from the reversal of plastic deformation in the larger grain. The driving force for this reverse deformation arises from the internal stresses built up during loading. Furthermore, the onset of dislocation activity in the larger grain coincides with the deviation of the stress–strain response from elastic behavior, revealing the microscopic details of the observed Bauschinger effect. We note that dislocation activity was also observed in the large grain during the first and second unloadings, confirming the repeatability of the observed phenomenon.

4.2. In situ TEM deformation of aluminum film with homogeneous microstructure

The stress–strain response of the aluminum film during in situ TEM deformation is shown in Fig. 2b. As evident from the figure, the aluminum film showed a markedly different stress–strain response compared to the gold film. Similar to the gold film, dislocation activity initiated in the relatively larger grains and progressively more grains deformed plastically with increasing strain. However, in contrast to the gold film, in both cycles a small increment in the applied strain (≈0.35%) was sufficient to induce macroscopic plasticity after the observation of the first dislocation activity. Fig. 5 shows the changes in the microstructure at ≈0.8% applied strain, during the first loading cycle (for the corresponding movie see Video S3). As evident from the figure, dislocation activity was observed in a majority of grains, with even some very small grains showing noticeable activity. Furthermore, the stress–strain slope at this point was already about one-tenth of the elastic modulus, confirming that plastic flow had initiated in most of the grains.

The behavior of the aluminum film during unloading was also dissimilar to the gold film, with hardly any dislocation activity observed in any of the grains. At the very end of the second unloading, however, a few discrete dislocation jumps could be observed in a large grain (see Video S4). The elastic nature of unloading is borne out by the macroscopic stress–strain response, which, apart from the small deviation at the end of the second unloading, shows a nearly perfect linear elastic behavior. The absence of Bauschinger effect is unsurprising since the build-up of internal stress during loading is greatly reduced by the relatively homogeneous nature of deformation. We note that

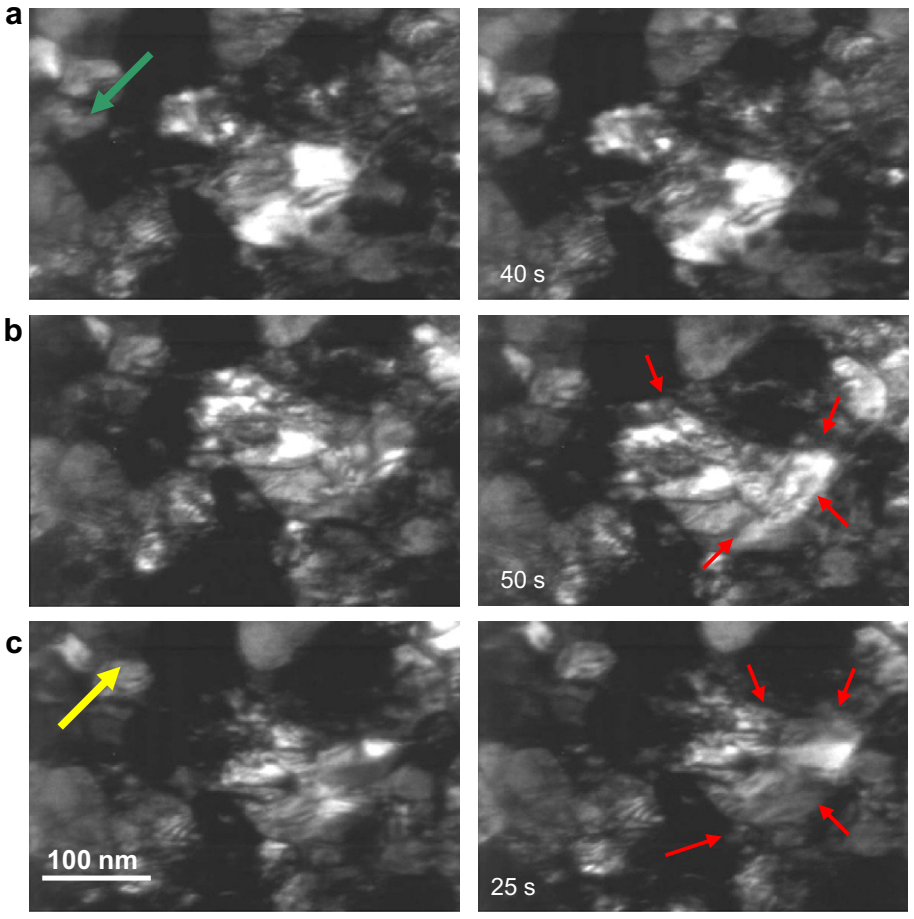

Fig. 4. The evolution of microstructure of the gold film during the different stages of the third deformation cycle. Figs. (a)–(c) correspond to the stages a–c indicated in Fig. 2a, respectively. Green and yellow arrows indicate the direction of loading and unloading, respectively. The figure on the left side shows the microstructure just before the application of the displacement pulses at each stage. The figure on the right side shows the microstructure after the application of the displacement pulses. The time difference is indicated in the right side figures. Clear changes in contrast (indicated by red arrows) were observed in the later stages of both loading (b) and unloading (c). On the other hand, very few changes in dislocation contrast were observed during the early stages of loading (a) as well as unloading. (For interpretation of the references to colour in this figure legend, the reader is referred to the web version of this article.)

there was no stress-assisted grain growth in this aluminum film during deformation, unlike the films in Ref. [12], possibly because of the columnar structure of the grains as well as the small applied strain. However, we observed grain growth in another aluminum film with a smaller grain size ($d_m = 100$ nm) when it was deformed to about 6% strain (data not shown).

4.3. Deformation of aluminum film with heterogenous microstructure

In addition to in situ TEM experiments, we also performed ex situ deformation experiments on another aluminum film. This aluminum film had a thickness (215 nm) and mean grain size (140 nm) similar to those of the aluminum film described in Section 4.2. However, in contrast to the highly textured aluminum film, this film did not have any preferred out-of-plane or in-plane texture (Fig. 6a). This non-textured film was synthesized by sputter depositing aluminum on a Si (0 0 1) wafer with the native oxide layer intact. The oxide layer disrupts the epitaxial growth and, as a result, the aluminum film does not have any preferred texture. The stress–strain response of this non-textured aluminum film is shown in Fig. 6c. As evident from the figure, this microstructurally heterogeneous aluminum film showed a gradual elastic–plastic transition and a substantial Bauschinger effect during unloading. These results clearly show that differences in microstructural heterogeneity alone can cause significant variation in the deformation behavior of nanocrystalline metals even if they have similar mean grain sizes.

5. Discussions

As mentioned earlier, nanocrystalline metals are expected to deform heterogeneously [38] and only a small fraction of grains undergo plastic events at the conventionally defined macroyield point [39]. To account for the extended microplasticity and to map the elastic–plastic transition in such heterogeneously deforming materials, a tangent

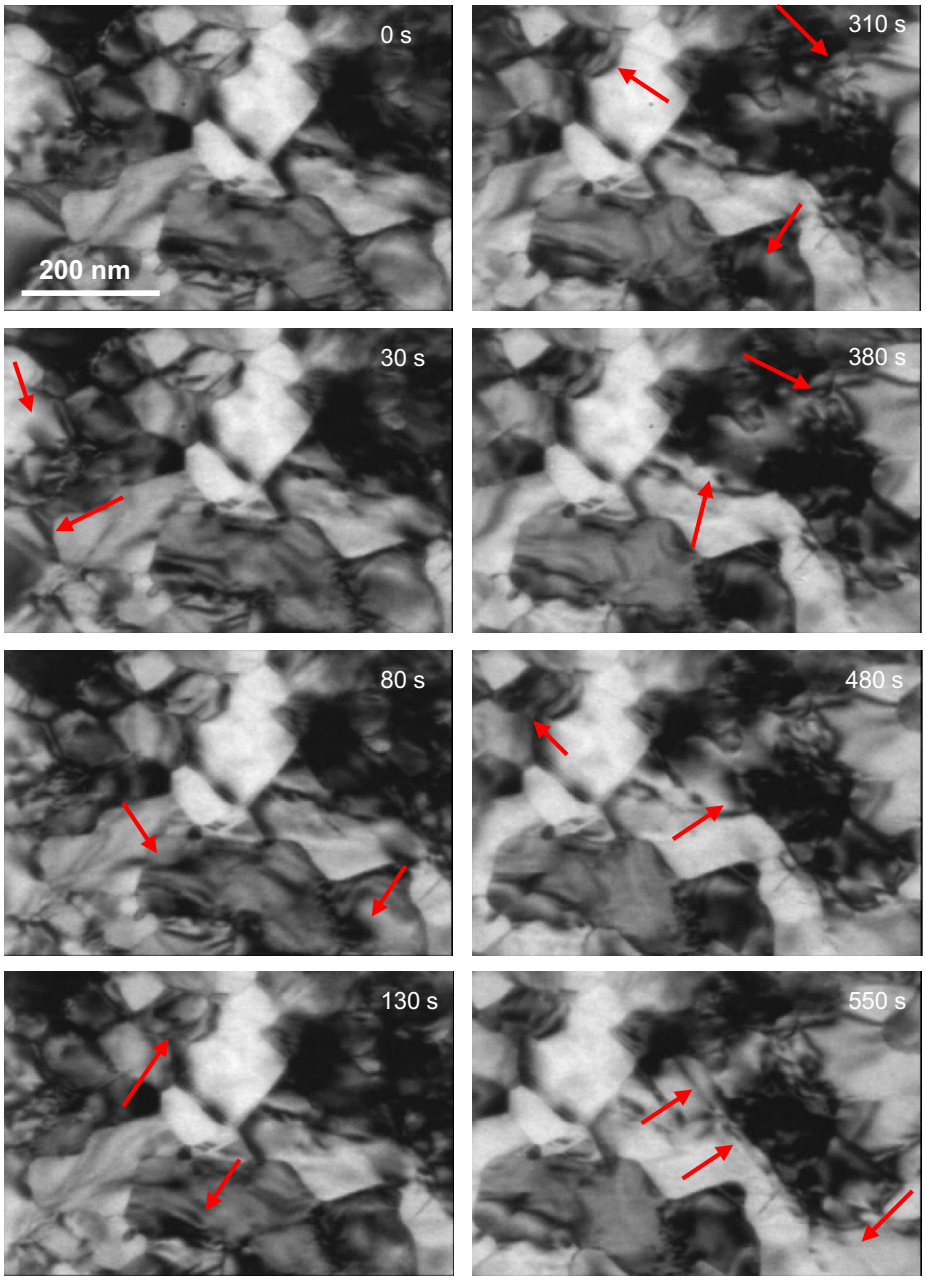

Fig. 5. The time evolution of the microstructure of the aluminum film at about 0.8% applied strain (first loading cycle). Dislocation activity could be seen in most of the grains at this stage (for the corresponding movie see Video S3).

modulus-based approach was developed. This method was used to analyze the deformation of Cu–Cr composite wires [24], and was later extended to thin films and multilayers [25]. Based on this analysis, it was concluded that the microdeformation stage in most fine-grained polycrystals greatly exceeded the 0.2% strain criterion.

Recently, the deformation behavior of Cu/Nb composite wires was examined in a series of studies [40–42] through a combination of macroscopic tensile experiments and in situ diffraction experiments. The Cu/Nb wires nominally consisted of three "phases" – a large-Cu phase, comprising grains ranging from a few hundred nanometers to several microns; a fine-Cu phase, comprising grains of a few tens to a few hundred nanometers; and Nb nanotubes/nanofilaments – and showed a macroscopic Bauschinger effect during unloading. The analysis of the in situ experiments using the tangent modulus approach revealed the presence of phase-specific elasto-plastic regimes and showed that the Bauschinger effect is the result of macroscopic yielding of the large-Cu phase in compression during unloading [26]. Furthermore, it was found that the elastic strain to total strain ratio in the large-Cu phase at its macroscopic yielding, in both tension and compression, was 0.33. Based on this insight, it was proposed that the macroyield stress be

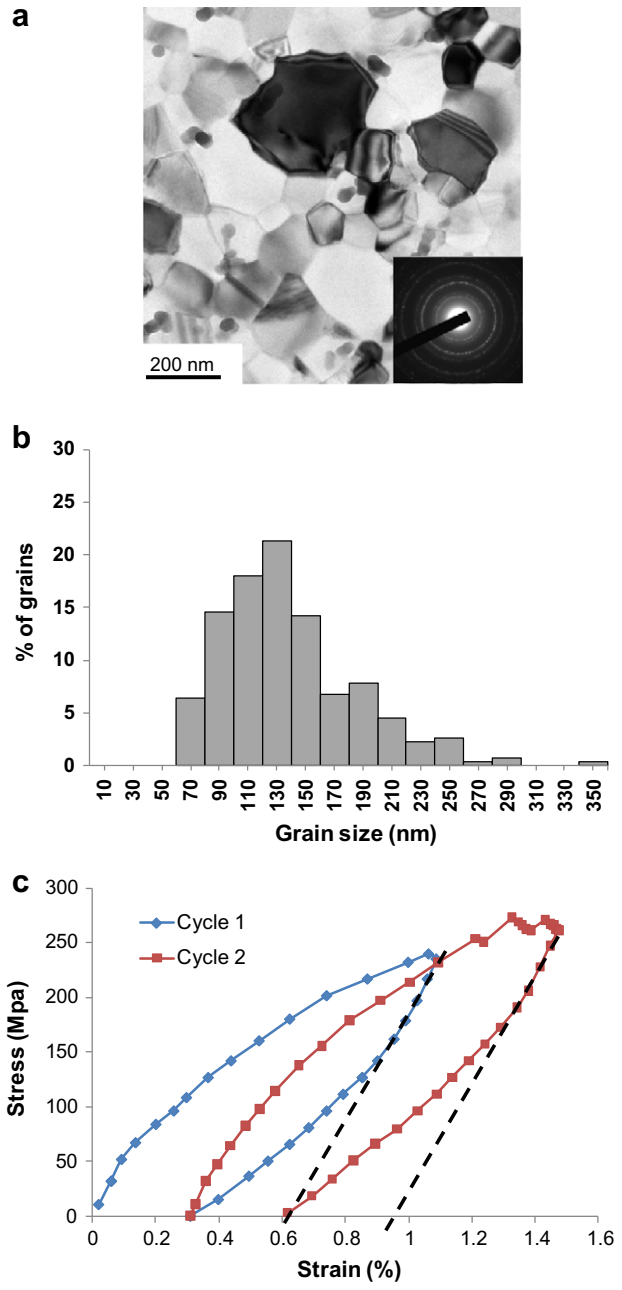

Fig. 6. Bright-field transmission electron micrograph (a) and histogram of grain sizes (b) of the non-textured aluminum film (thickness 215 nm, $d_m = 140$ nm). The diffraction pattern (shown as the inset in (a)) reveals the lack of any preferred texture. (c) Stress–strain measurements for the aluminum film during two cycles. The film shows a gradual elastic–plastic transition during loading and a substantial Bauschinger effect during unloading. The elastic unloading path is indicated by the dashed black lines.

defined as the point at which the macroscopic work hardening rate (tangent modulus), $\theta = d\sigma/d\epsilon$, becomes less than one-third of the Young's modulus.

The tangent modulus approach to determine the macro-yield point of nanocrystalline metals is intuitively appealing since it takes into account their gradual elastic–plastic transition. Our in situ TEM experiments suggest that a criterion for macroplastic transition should take into account an additional factor, namely the heterogeneity of the microstructure. The microstructurally heterogenous gold film undergoes only microplastic deformation in all three cycles and as a result shows a pronounced Bauschinger effect. This is the case even at the end of the third loading, where the macroscopic work hardening rate is less than one-quarter of the Young's modulus. On the other hand, the microstructurally homogeneous aluminum film, despite having a comparable mean grain size, exhibits a fairly sharp elastic–plastic transition – an increment in applied strain of around 0.35% after the onset of microplasticity is sufficient to induce macroplasticity in both cycles. This transition to macroplasticity is confirmed by the reduction in the macroscopic work hardening rate to about one-tenth of the Young's modulus. We also performed additional in situ TEM straining experiments on other Al films with homogeneous microstructure to verify the observations reported here. These studies unambiguously confirmed that a relatively homogenous microstructure leads to a reduction in microplastic deformation as well as Bauschinger effect during unloading.

The effect of an inhomogeneous microstructure on the stress–strain response can be understood in terms of the simple one-dimensional model shown in Fig. 7a. The model idealizes the microstructure as a collection of grains of different sizes, all of which are under the same strain (equal to the macroscopic strain) at any point during loading or unloading. An equivalent representation of such a microstructure in terms of springs and sliding elements is shown in Fig. 7b. Each spring–slider pair represents a grain. The extension of the springs represents elastic deformation in the grains while the motion of the sliders represents plastic deformation. All the springs have equal stiffness, but greater force is required to move larger sliding elements. In effect, spring–slider pairs with larger sliding elements represent grains with high yield stress and vice versa. To calculate the uniaxial stress–strain response of such a system, we further assume that

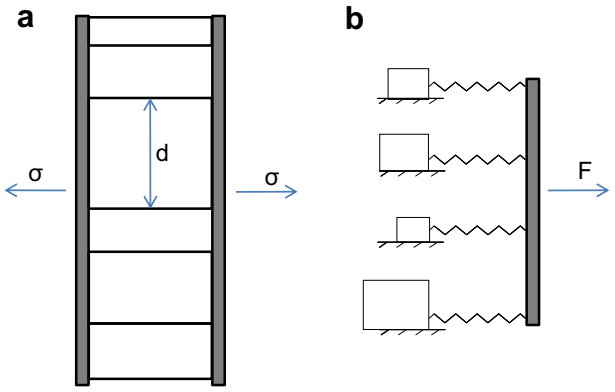

Fig. 7. (a) Idealized microstructure used for modeling the effect of microstructural heterogeneity. (b) Equivalent representation of the microstructure in terms of springs and sliding elements. Each spring–slider pair represents a grain. The pairs with larger sliding elements represent grains with high yield stress and vice versa.

1. The grains have the stress–strain characteristics of an elastic–perfectly plastic material, that is, there is no strain hardening.
2. The yield stress of the grains is the same in both tension and compression.

Based on these assumptions, the normal stress increment in grain i due to a macroscopic strain increment $d\epsilon$ during loading is given by

$$d\sigma_i = \begin{cases} Ed\epsilon & \sigma_i < \sigma_{yi} \\ 0 & \sigma_i \geqslant \sigma_{yi} \end{cases} \quad (1)$$

Here σ_{yi} is the tensile yield stress of grain i and E is the Young's modulus. The stress decrement in grain i due to a macroscopic strain decrement during unloading is given by

$$d\sigma_i = \begin{cases} Ed\epsilon & \sigma_i > -\sigma_{yi} \\ 0 & \sigma_i \leqslant -\sigma_{yi} \end{cases} \quad (2)$$

The macroscopic stress at any point during loading or unloading is given by the weighted average of the stresses in the individual grains. Therefore,

$$\sigma = \frac{\sum \sigma_i d_i}{\sum d_i} \quad (3)$$

where d_i is the size of grain i. We now use this simple model to simulate the uniaxial stress–strain response of the 225 nm thick textured aluminum film (Fig. 2b) and the 215 nm thick non-textured aluminum film (Fig. 6c). In these simulations, we use the actual grain size distribution of the films shown in Fig. 1d and Fig. 6b, respectively.

To simulate the stress–strain response, we first assign yield stresses to individual grains in the following way. Since the mean grain sizes (d_m) of these films fall in the nanocrystalline transition regime (around 100 nm), we assume that grains that are larger than d_m have pre-existing dislocation sources, the size of which scale as the grain size. Since the shear stress required to activate a dislocation source is inversely proportional to its size, the critical resolved shear stress for these grains is inversely proportional their size d_i. However, the stress at which a grain yields also depends on its orientation with respect to the straining direction, i.e. the Schmid factor (m) of the slip systems in the grain. Typically, m is different for different slip systems and the system with the highest m gets activated first. However, depending on the grain orientation, up to five independent slip systems may be required to accommodate the imposed strain purely through slip [1]. For simplicity, we therefore assume that a grain yields only when the applied stress is sufficient to activate at least five slip systems in the grain. If fewer than five slip systems have a non-zero m, we assume that the grain yields when the least favorable system is activated. Hence, the yield stress of the grains is dictated by the m of the least favorable slip system required to accommodate the imposed strain.

For grains smaller than d_m we assume that plasticity is controlled by nucleation of dislocations from grain boundaries and is independent of the grain size. Therefore, we assign yield stress values for these smaller grains randomly from a uniform distribution with a lower limit of σ_{nl} and an upper limit of σ_{nu}.

We first consider the textured Al film which has only two major grain orientations. The grains whose [0 0 1] direction is aligned with the loading axis have eight slip systems with non-zero m. The other set of grains have four such slip systems. However, the Schmid factor of all the slip systems in both sets of grains is identical ($m_t = 0.408$). Therefore, the uniaxial yield stress of grains larger than d_m (120 nm) can be represented simply by

$$\sigma_{yi} = \frac{C}{m_t d_i} \quad d_i > 120 \text{ nm} \quad (4)$$

where C is a constant. The non-textured film has a slightly larger mean grain size ($d_m = 140$ nm) and the orientation of the grains vary. Therefore, for the non-textured film

$$\sigma_{yi} = \frac{D}{m_i d_i} \quad d_i > 140 \text{ nm} \quad (5)$$

where D is a constant and m_i is the Schmid factor associated with grain i. Since the grains are randomly oriented, we chose m_i from a uniform distribution with a range of 0.1–0.4. The limits 0.1 and 0.4 are conservative since there are grain orientations for which the m of the least favorable slip system is outside these limits. The macroscopic stress–strain response is then calculated using Eqs. (1)–(3). Fig. 8 shows the typical response for the textured and non-textured film obtained from the simulations. For both the films, approximately 12,000 grains were used for simulating the stress–strain behavior. For these simulations, $C = 10$ N/m, $D = 5$ N/m, $\sigma_{nl} = 250$ MPa and $\sigma_{nu} = 750$ MPa. These values were chosen so that the maximum stress obtained in the simulations was similar to the experiments. Changing these parameters leads to variation in the magnitude of the calculated stresses, but the qualitative stress–strain response remains similar.

As evident from Fig. 8, the textured film shows very little Bauschinger effect during both the cycles, which is consistent with the experimentally observed response (Fig. 2b). This is the case because, even though there is variation in σ_y among the grains due to their size, it is sufficient to induce reverse yielding in only a few larger grains during unloading. On the other hand, the non-textured film shows a noticeable Bauschinger effect in both cycles, which is consistent with the experimentally observed behavior (Fig. 6c). In the non-textured film, the variation in σ_y comes from both the grain size and the orientation (m). This leads to a substantially more heterogeneous stress distribution during loading. As a result, reverse yielding occurs in a significant fraction of large/favorably oriented grains during unloading, leading to a substantial Bauschinger effect.

Note that the stress–strain curves shown in Fig. 8 corresponds to a particular simulation. Because the yield stresses

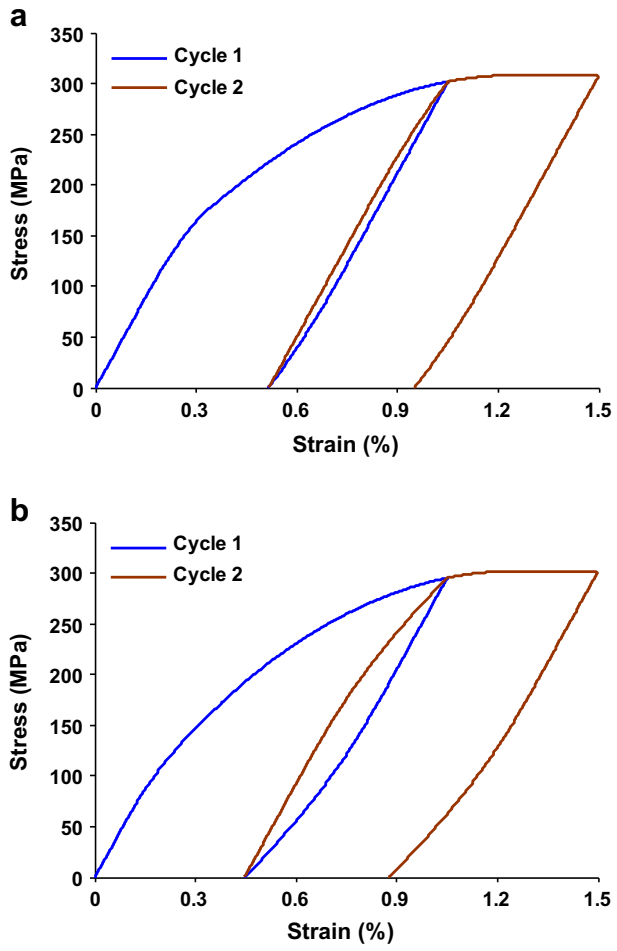

Fig. 8. Simulated stress–strain curves for the 225 nm thick textured Al film (a) and the 215 nm thick non-textured Al film (b). The textured film shows only a small Bauschinger effect in both cycles, whereas the non-textured film shows a substantial Bauschinger effect.

of grains smaller than d_m are assigned randomly, there is a very small variation in the response from simulation to simulation. In the case of the non-textured film there is a slightly larger variation, since the yield stress of larger grains is also chosen randomly (Eq. (5)). Typically, the Bauschinger effect is most pronounced in the non-textured film when the relatively larger grains have high m and vice versa. However, the overall response is very similar from simulation to simulation. In addition, as the number of grains used in the simulations becomes higher the variation becomes negligible.

In this simple model, only variations in yield stress arising from the distribution of grain sizes and orientation were considered. However, in real experimental samples yielding in different grains can be affected, among other factors, by differences in the grain boundary structure and density of pre-existing dislocations, and therefore a more heterogeneous stress distribution is likely. Also, grains may have lower yield stress in compression if they have deformed plastically in tension. Both these effects will lead to a more pronounced Bauschinger effect. Despite the many simplifying assumptions used, the model captures the effect of microstructural heterogeneity on the stress–strain response reasonably well. Along with the insights provided by the in situ TEM observations, these results clearly demonstrate the critical role of heterogeneity in shaping the mechanical behavior of nanocrystalline metals.

6. Conclusions

In this study, we performed quantitative in situ TEM straining experiments on free-standing gold and aluminum films to explore the role of microstructural heterogeneity in the deformation behavior of nanocrystalline metals. The gold film, which has a fairly heterogenous microstructure, with randomly oriented grains and a wide distribution of grain sizes, showed extensive microplasticity and a pronounced Bauschinger effect during unloading. Similar behavior was also seen in aluminum films with a heterogeneous microstructure. Microstructurally homogeneous aluminum films, in contrast, exhibited limited microplastic deformation and a very small Bauschinger effect despite a comparable mean grain size. A simple model that incorporate the heterogeneity of the microstructure was used to simulate the stress–strain behavior of the aluminum films. The simulations confirmed that the extended microplasticity and Bauschinger effect are the result of an inhomogeneous stress distribution (high stresses in elastically deforming grains, low stresses in plastically deforming grains) caused by microstructural heterogeneity. These results strongly argue against a purely grain size-centric description of plasticity in nanocrystalline metals and emphasize the need to take into account both the microstructural size and the heterogeneity.

Acknowledgements

This material is based upon work supported by the National Science Foundation under Award No. NSF ECS-0304243 and Award No. NSF CMMI-0728189. The gold and aluminum specimens were fabricated in the Micro-nano-mechanical Systems Cleanroom and Micro Nano Technology Laboratory at the University of Illinois at Urbana-Champaign. The in situ TEM experiments were performed at the University of Vienna, supported by the research focus “Materials Science – Functional Materials and Nanostructures”. We thank Prof. Hael Mughrabi (University of Erlangen) for valuable discussions.

Appendix A. Supplementary material

Supplementary data associated with this article can be found, in the online version, at doi:10.1016/j.actamat.2010.05.013.

References

[1] Hirth JH, Lothe J. Theory of dislocations. New York: Wiley-Interscience; 1982.

[2] Legros M, Elliot BR, Rittner MN, Weertman JR, Hemker KJ. Philos Mag A 2000;80:1017–26.
[3] Haque MA, Saif MTA. J Mater Res 2005;20:1769–77.
[4] Lu L, Sui ML, Lu K. Science 2000;287:1463–6.
[5] Legros M, Gianola DS, Hemker KJ. Acta Mater 2008;56:3380–93.
[6] Wu XL, Zhu YT, Ma E. Appl Phys Lett 2006;88:121905.
[7] Wang YB, Li BQ, Sui ML, Mao SX. Appl Phys Lett 2008;92:011903.
[8] Meyers M, Mishra A, Benson D. Prog Mater Sci 2006;51:427–556.
[9] Schwaiger R, Moser B, Dao M, Chollacoop N, Suresh S. Acta Mater 2003;51:5159–72.
[10] Wang YM, Hamza AV, Ma E. Acta Mater 2006;54:2715–26.
[11] Zhang K, Weertman JR, Eastman JA. Appl Phys Lett 2005;87:061921.
[12] Gianola DS, Van Petegem S, Legros M, Brandstetter S, Van Swygenhoven H, Hemker KJ. Acta Mater 2006;54:2253–63.
[13] Schiotz J, Jacobsen KW. Science 2003;301:1357–9.
[14] Yamakov V, Wolf D, Phillpot SR, Mukherjee AK, Gleiter H. Nat Mater 2004;3:43–7.
[15] Swygenhoven HV, Derlet PM, Froseth AG. Nat Mater 2004;3:399–403.
[16] Swygenhoven HV. Mater Sci Eng A 2008;483–484:33–9.
[17] Hugo RC, Kung H, Weertman JR, Mitra R, Knapp JA, Follstaedt D. Acta Mater 2003;51:1937–43.
[18] Kumar KS, Suresh S, Chisholm MF, Horton JA, Wang P. Acta Mater 2003;51:387–405.
[19] Robertson IM, Ferreira P, Dehm G, Hull R. MRS Bull 2008;33/2:122–31.
[20] Oh SH, Legros M, Kiene D, Gruber P, Dehm G. Acta Mater 2007;55:5558–71.
[21] Kumar KS, Van Swygenhoven H, Suresh S. Acta Mater 2003;51:5743–74.
[22] Brandstetter S, Swygenhoven HV, Petegem SV, Schmitt B, MaaB R, Derlet PM. Adv Mater 2006;18:1545–8.
[23] Li H, Choo H, Ren Y, Saleh TA, Lienert U, Liaw PK, et al. Phys Rev Lett 2008;101:015502.
[24] Sinclair CW, Saada G, Embury JD. Philos Mag 2006;86:4081–98.
[25] Saada G, Verdier M, Dirras GF. Philos Mag 2007;87:4875–92.
[26] Thilly L, Petegem SV, Renault P-O, Lecouturier F, Vidal V, Schmitt B, et al. Acta Mater 2009;57:3157–69.
[27] Valiev R, Islamgaliev R, Alexandrov I. Prog Mater Sci 2000;45:103–89.
[28] Lonardelli I, Almer J, Ischia G, Menapace C, Molinari A. Scr Mater 2009;60:520–3.
[29] Li X, Wei Y, Yang W, Gao H. Proc Natl Acad Sci USA 2009;106:16108–13.
[30] Rajagopalan J, Han JH, Saif MTA. Science 2007;315:1831–4.
[31] Rajagopalan J, Han JH, Saif MTA. Scr Mater 2008;59:921–6.
[32] Rajagopalan J, Han JH, Saif MTA. Scr Mater 2008;59:734–7.
[33] Han JH, Saif MTA. Rev Sci Instrum 2006;77:045102.
[34] Haque MA, Saif MTA. Expt Mech 2002;42:123–8.
[35] Rentenberger C, Waitz T, Karnthaler HP. Scr Mater 2004;51:789–94.
[36] Niwa H, Kato M. Appl Phys Lett 1991;59:543–5.
[37] Van Swygenhoven H, Derlet PM, Froseth A. Acta Mater 2006;54:1975–83.
[38] Bitzek E, Derlet P, Anderson P, Swygenhoven HV. Acta Mater 2008;56:4846–57.
[39] Saada G. Mater Sci Eng A 2005;400–401:146–9.
[40] Thilly L, Renault P-O, Vidal V, Lecouturier F, Petegem SV, Stuhr U, et al. Appl Phys Lett 2006;88:191906.
[41] Thilly L, Renault PO, Petegem SV, Brandstetter S, Schmitt B, Swygenhoven HV, et al. Appl Phys Lett 2007;90:241907.
[42] Vidal V, Thilly L, Petegem SV, Stuhr U, Lecouturier F, Renault P-O, et al. Scr Mater 2009;60:171–4.